European Journal of Mechanics / A Solids 115 (2026) 105779

Contents lists available at ScienceDirect

European Journal of Mechanics / A Solids

journal homepage: www.elsevier.com/locate/ejmsol

Full length article

# Modeling the mechanical behavior of coated masonry elements using surface stress theory

Simona Di Nino [a], Giuseppe Rosi [b], Francesco D'Annibale [a,c,*]

[a] Department of Civil, Construction-Architectural and Environmental Engineering, University of L'Aquila, 67100 L'Aquila, Italy
[b] Univ Paris Est Creteil, Univ Gustave Eiffel, CNRS, UMR 8208, MSME, F-94010 Créteil, France
[c] International Research Center on Mathematics and Mechanics of Complex Systems, University of L'Aquila, 67100 L'Aquila, Italy

ARTICLE INFO

*Keywords:*
Masonry
Steel Fiber Reinforced Mortar
Surface Stress Model
Static and dynamic Finite Element analyses

ABSTRACT

The Gurtin–Murdoch Surface Stress Model (SSM) is employed to model thin coatings of Steel Fiber Reinforced Mortar (SFRM) applied to masonry structures. This approach introduces a non-classical mechanical boundary condition, which expresses in-plane surface traction on the masonry facades in terms of surface stress and inertia. Finite Element (FE) analyses are performed within the elastic regime on coated masonry wall samples, both under static and dynamic loading conditions, to validate the accuracy of the theoretical model. Finally, a more realistic masonry structural system is analyzed to demonstrate the effectiveness of the proposed reinforcement and highlight the computational efficiency of the proposed surface model.

## 1. Introduction

The inherent low tensile strength of masonry often necessitates the implementation of reinforcement measures in such structures (Como, 2013). Several technologies have been developed for strengthening and rehabilitating this kind of buildings. A detailed description of existing reinforcement methods is not provided here; instead, readers are referred to specific articles, such as Bhattacharya et al. (2014) and Wang et al. (2018), where most interventions are thoroughly covered. These include techniques like shotcrete (Shabdin et al., 2018), Textile Reinforced Mortar (TRM) (Kouris et al., 2018), Fiber Reinforced Polymers (FRPs) (Gattesco et al., 2015), Fiber Reinforced Cementitious Matrix (FRCM) (Angiolilli et al., 2020).

On the other hand, in this paper the interest is on an alternative technique based on the use of Steel Fiber Reinforced Mortar (SFRM). It involves the application of thin SFRM coatings, either on one or both sides of masonry walls. This technology offers several advantages, such as the time-saving associated with constructing thin coatings and enhanced crack control due to the steel fibers in the mortar. Over the past decade, this retrofitting method has gained significant attention in the academic field, primarily through experimental tests demonstrating its effectiveness in enhancing both the bearing capacity and stiffness of masonry walls, whether newly constructed or already damaged (Sevil et al., 2011; Facconi et al., 2015; Messali et al., 2017; Simoncello et al., 2019; Facconi et al., 2020; Lucchini et al., 2020; Zampieri et al., 2020; Yu and Park, 2020; Buyukkaragoz and Kopraman, 2021; Lucchini et al., 2023). Among them, in Facconi et al. (2015), quasi-static reverse cyclic tests are carried out on full-scale masonry shear walls, which are either strengthened or repaired using thin coatings of SFRM containing nano-silica. In Lucchini et al. (2020), uniaxial and diagonal compression tests are performed on masonry samples retrofitted with SFRM coating. In Zampieri et al. (2020) the bond behavior of SFRM applied onto masonry substrates is investigated through double shear lap tests. However, in practice, this reinforcement technique is often applied empirically, without a comprehensive quantitative assessment of its effectiveness. This is primarily due to the lack of accurate and widely accepted equivalent models, as well as the increased computational cost associated with finite element modeling of the coatings—particularly in two main scenarios: (i) in the worst-case scenario, where solid elements are employed to capture through-thickness behavior, leading to very fine meshes and high computational demand; and (ii) in a more efficient scenario, where membrane elements are used, which adequately capture in-plane behavior but sacrifice through-thickness information. Even if the latter can offer a computationally lighter alternative, it necessitates the explicit definition of additional finite elements, interface conditions, and a dedicated meshing strategy. Especially, the literature includes relatively few attempts to model this technology, such as Lucchini et al. (2020), Zampieri et al. (2020), Buyukkaragoz and Kopraman (2021), Facconi et al. (2023) and Lucchini et al. (2023), most of which involve detailed Finite Element (FE) models that replicate experimental tests. More recently, in line with the trend towards macro-modeling of masonry structures (Di Nino et al., 2017; Di Nino

* Corresponding author at: Department of Civil, Construction-Architectural and Environmental Engineering, University of L'Aquila, 67100 L'Aquila, Italy.
*E-mail addresses:* simona.dinino@univaq.it (S. Di Nino), giuseppe.rosi@u-pec.fr (G. Rosi), francesco.dannibale@univaq.it (F. D'Annibale).

https://doi.org/10.1016/j.euromechsol.2025.105779
Received 2 January 2025; Received in revised form 13 June 2025; Accepted 4 July 2025
Available online 16 July 2025

and Zulli, 2020; Di Nino, 2022), some analytical models have been developed (Facconi et al., 2023; Di Nino and Luongo, 2023, 2024), limited to the in-plane behavior of these structure. Among them, in Di Nino and Luongo (2023, 2024), a two-step homogenization approach is introduced. It builds on the methods and philosophy developed in Di Nino and Luongo (2019) for unreinforced masonry, extending them to coated masonry under in-plane loads. As a result, simple closed-form expressions are derived for the (membrane) macroscopic elastic constants of an equivalent homogeneous and orthotropic Cauchy continuum. On the other hand, the literature suggests that conventional continuum models are inadequate for accurately capturing the out-of-plane behavior of layered structures, such as coated walls. In such cases, more advanced equivalent models are required, like the Cosserat continuum (e.g., Biot, 1967; Sun et al., 1968; Zvolinskii and Shkhinek, 1984; Adhikary and Dyskin, 1997). Unlike traditional solid mechanics, where stress and strain are typically assumed to act at points without accounting for rotational effects, the Cosserat continuum introduces additional degrees of freedom, allowing for the modeling of both translations and rotations of material elements. This model has also been applied to unreinforced masonry (e.g., Masiani and Trovalusci, 1996; Trovalusci and Masiani, 2003; Salerno and De Felice, 2009; Stefanou et al., 2008; Addessi et al., 2010), where the discrete nature of blocks and joints can induce behaviors such as micro-rotations and sliding. However, the drawback of these models is that they are typically not easily implementable in structural analysis software.

This article proposes an alternative approach to model both the in-plane and out-of-plane behavior of masonry structures reinforced with thin SFRM coatings, striking a balance between detailed FE models and simplified ones. It involves: (i) developing detailed three-dimensional finite element models for unreinforced masonry, and (ii) incorporating material surfaces or "surface stresses" to account for the SFRM coatings. To address this issue, the Surface Stress Model (SSM), developed by Gurtin and Ian Murdoch (1975) and Gurtin and Murdoch (1978), is used. The model employs non-classical boundary conditions that give the surface traction on the substrate in terms of in-plane surface stress and inertia. It effectively captures surface stress effects without the need for explicit fine-mesh modeling of SFRM coatings, thereby reducing computational costs, while maintaining accuracy. This theory is particularly relevant in scenarios where a body surface is coated with a thin layer of another material. Despite its ancient origins, the SSM continues to be widely utilized today, especially in nanomechanics, where the surface effects play an relevant role. Below, some key applications of the Gurtin–Murdoch model in engineering are highlighted. One prominent area of application involves describing the mechanical behavior of nanostructured elements (Wang et al., 2011), including nanowires (e.g., Wang et al., 2021), nanobeams (e.g., Eltaher et al., 2013; Preethi et al., 2018), nanofilms (e.g., Zhao and Rajapakse, 2013), and nanoscale plates and shells (e.g., Dahmen et al., 2000; Eremeyev et al., 2009; Altenbach et al., 2010; Altenbach and Eremeyev, 2011). In this context, particular attention has been given to investigating the impact of surface stress on wave propagation in solids (Gurtin and Murdoch, 1976; Eremeyev et al., 2016, 2019, 2020). Efforts have also been made to extend the model to account for inelastic behavior, such as surface viscoelasticity phenomena (e.g., Altenbach et al., 2012; Eremeyev, 2024). Another critical field of research concerns the application of the SSM to analyze nanocomposite materials and interfaces (e.g., Kushch et al., 2013; Nazarenko et al., 2016; Shiva et al., 2019; Mogilevskaya et al., 2021), with investigations focusing on enhancing delamination resistance and optimizing structural stability (e.g., Lu et al., 2011). Furthermore, the SSM has found applications in the development of micro-electromechanical systems (MEMS) and nano-electromechanical systems (NEMS), aiming to improve the precision of mechanical response predictions (e.g., Shaat and Mohamed, 2014). Recently, there has been growing interest in utilizing surface elasticity in the design of advanced materials, such as metamaterials engineered with micro- or nanoscale architectures (e.g., Nasedkin and Kornievsky, 2019).

However, the Gurtin–Murdoch model is rarely applied in traditional civil engineering, which primarily focuses on macroscopic structures such as masonry buildings. The novelty of this study lies in its pioneering application to large-scale structures, yielding unexpectedly positive results. There are no inherent limitations preventing the application of this model in traditional civil engineering. However, its limited adoption is likely due to the lack of direct integration into conventional structural analysis software. In this regard, this work could be a valuable first step towards incorporating this model into commercial civil engineering software. The primary advantages include: (a) a significant reduction in computational costs, enabling much faster analyses compared to detailed finite element models; (b) the ability to easily integrate reinforcement layers into existing FE models, without the need for complex remeshing or new model development. This last aspect is particularly beneficial when working with complex geometries, such as church facades, where pre-existing models can be used to assess the feasibility of applying SFRM layers for reinforcement.

Even though masonry exhibits nonlinear behavior even at low load levels, all analyses in this study are conducted in the elastic regime. This choice is primarily driven by the goal of assessing the feasibility and effectiveness of the SSM for SFRM coatings on masonry structures. Experimental findings (e.g., Facconi et al., 2015) support the validity of elastic analysis, showing that strengthened specimens exhibit significantly higher initial stiffness and delayed crack formation compared to unreinforced walls. Furthermore, while SFRM coatings can enhance the stiffness and strength of masonry walls — potentially improving their seismic performance — they may also lead to increased seismic demand due to changes in the dynamic properties of the structure, such as a reduction in the fundamental period. It is therefore essential to assess these effects through elastic dynamic analyses.

The structure of the paper is organized as follows. In Section 2, the SSM of Gurtin–Murdoch is briefly revisited using a direct approach. In Section 3, static and dynamic (modal) FE analyses are performed within the elastic regime on models of coated masonry wall samples to assess the accuracy of the theoretical model. In Section 4, several numerical applications are conducted to investigate (i) the effectiveness of the SFRM coating on both undamaged and damaged masonry, and (ii) the computational advantages of the model in terms of solution time. Finally, Section 5 summarizes the key findings of the work and outlines potential future developments. The paper concludes with an Appendix that illustrates the variational approach to SSM.

## 2. Surface Stress Model (SSM) of Gurtin–Murdoch

This section revisits and summarizes the mechanical theory of the Gurtin–Murdoch Surface Stress Model (SSM), as presented in Gurtin and Ian Murdoch (1975) and Gurtin and Murdoch (1978), to ensure consistency with the work. The direct formulation is described first, followed by a brief explanation of the variational approach in Appendix. Additionally, a straightforward method for determining the equivalent stiffness and mass properties of the material surface is provided. Notably, the inclusion of the variational approach is driven by practical considerations, as this formulation will later be integrated into finite element (FE) analyses, as will become clear in subsequent sections.

### 2.1. Direct approach

A three-dimensional body occupying the volume $\mathscr{D}_1$ is considered, with a surface region coated by a thin layer of another material, occupying the volume $\mathscr{D}_2$. The latter is modeled as a material surface $\mathscr{S}$, consisting of the interface between $\mathscr{D}_1$ and $\mathscr{D}_2$, i.e., $\mathscr{S} = \mathscr{D}_1 \cap \mathscr{D}_2$, having the outward unit normal $\mathbf{n}$ (see the scheme in Fig. 1). This surface behaves as an equivalent membrane, endowed with a

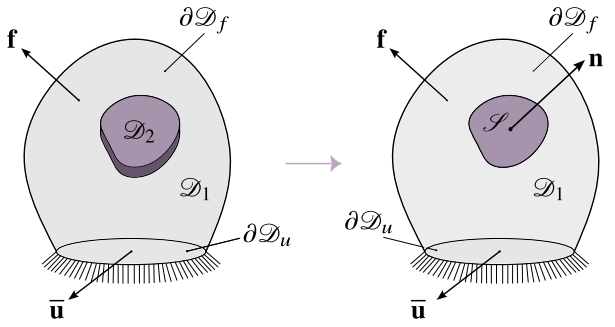


**Fig. 1.** Three-dimensional modeling of a Cauchy body endowed with a material surface.

structure which reflects the behavior of the surface region. It is assumed that $\mathscr{S}$ adheres to $\mathscr{D}_1$ without slipping and that both $\mathscr{D}_1$ and $\mathscr{S}$ are homogeneous, linearly elastic, and isotropic. According to the Gurtin–Murdoch model (Gurtin and Murdoch, 1978), the equations of the elasto-dynamic problem consist of the classical volume equations:

$$\begin{aligned} &\mathrm{div}\mathbf{T} = \rho_1 \ddot{\mathbf{u}}, \\ &\mathbf{T} = \lambda_1 \mathrm{tr}\,(\mathbf{E})\,\mathbf{I} + 2\mu_1 \mathbf{E}, \quad \text{in } \mathscr{D}_1, \\ &\mathbf{E} = \frac{1}{2}\left(\nabla\mathbf{u} + \nabla\mathbf{u}^T\right), \end{aligned} \tag{1}$$

coupled with the surface equations:

$$\begin{aligned} &\mathbf{T}\mathbf{n} = \mathrm{div}_{\mathscr{S}}\mathbf{T}_s - \rho_s \ddot{\mathbf{u}}, \\ &\mathbf{T}_s = \lambda_s \mathrm{tr}\left(\mathbf{E}_s\right)\mathbf{P} + 2\mu_s \mathbf{P}\mathbf{E}_s, \qquad \text{in } \mathscr{S}, \\ &\mathbf{E}_s = \frac{1}{2}\left(\nabla_{\mathscr{S}}\mathbf{u}\cdot\mathbf{P} + \mathbf{P}\cdot\nabla_{\mathscr{S}}\mathbf{u}^T\right). \end{aligned} \tag{2}$$

In Eq. (1), $\mathbf{T}$, $\mathbf{u}$ and $\mathbf{E}$, denote, respectively, the stress, displacement and strain fields on $\mathscr{D}_1$; $\mathbf{I}$ is $3 \times 3$ identity matrix and the constants $\rho_1$ and $\lambda_1, \mu_1$ are the mass density and the Lamé moduli for $\mathscr{D}_1$. The operators div and $\nabla$ represent divergence and gradient, respectively, evaluated within the volume $\mathscr{D}_1$; the two dots indicate the second derivative with respect to time. Passing to Eq. (2), $\mathbf{T}_s$ is the *Surface Stress tensor*, representing the stress localized in the surface region $\mathscr{S}$, having the outward unit normal $\mathbf{n}$. It is related to the surface strain tensor $\mathbf{E}_s$ by the constitutive law Eq. (2)b, where $\mathbf{E}_s$ is defined as in Eq. (2)c, with:

$$\mathbf{P} = \mathbf{I} - \mathbf{n}\otimes\mathbf{n}, \tag{3}$$

the projection onto the tangent space of the surface $\mathscr{S}$. The operators $\mathrm{div}_{\mathscr{S}}$ and $\nabla_{\mathscr{S}}$ are the surface divergence and gradient, respectively. Accordingly, $\nabla_{\mathscr{S}}\mathbf{u} = \mathbf{P}\cdot\nabla\mathbf{u}$ and $\mathrm{div}_{\mathscr{S}}\mathbf{T}_s = \nabla_{\mathscr{S}}\cdot\mathbf{T}_s = \mathbf{P}\cdot\nabla\cdot\mathbf{T}_s$, from which $\mathbf{E}_s = \mathbf{P}\cdot\mathbf{E}\cdot\mathbf{P}$. The constants $\rho_s$ and $\lambda_s, \mu_s$ are the equivalent surface mass density and Lamé moduli of the material surface $\mathscr{S}$, that needs to be identified.

Finally, denoting with $\partial\mathscr{D}_u$ and $\partial\mathscr{D}_f$ the constraint and free boundary surfaces of $\mathscr{D}_1$, subjected respectively to prescribed displacements $\bar{\mathbf{u}}$ and external forces $\mathbf{f}$, the following boundary equations also hold:

$$\begin{aligned} &\mathbf{u} = \bar{\mathbf{u}}, \quad \text{in } \partial\mathscr{D}_u, \\ &\mathbf{T}\mathbf{n} = \mathbf{f}, \quad \text{in } \partial\mathscr{D}_f, \end{aligned} \tag{4}$$

with $\mathbf{n}$ the outward unit normal of the surface $\partial\mathscr{D}_f$.

The variational form of the theory is detailed in Appendix, as it is used for the numerical implementations of the model, which will be clarified later.

### 2.2. Identification of the stiffness and mass properties of the material surface

The equivalent properties of the material surface $\mathscr{S}$ are derived from the three-dimensional body $\mathscr{D}_2$. This body is assumed to be homogeneous and isotropic, with mass density $\rho_2$, Lamé moduli $\lambda_2, \mu_2$,

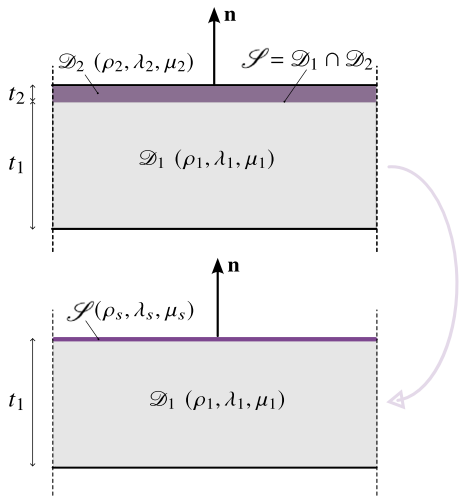


**Fig. 2.** Modeling scheme of a material surface with constant thickness in a cross-section parallel to its normal direction.

and with a uniform thickness $t_2$ across the interface $\mathscr{S}$. When $t_2$ is sufficiently small, $\mathscr{D}_2$ can be assumed in a "plane stress" condition, meaning that the stress state within the material is uniform across the thickness and stress gradients through the thickness can be ignored. Consequently, $\mathscr{D}_2$ behaves approximately as a two-dimensional membrane with negligible bending stiffness. Accordingly, the equivalent properties of $\mathscr{S}$ are obtained as follows (Altenbach et al., 2010):

$$\rho_s := \rho_2 t_2, \quad \lambda_s := \lambda_2 t_2, \quad \mu_s := \mu_2 t_2. \tag{5}$$

A modeling scheme is also provided in Fig. 2, illustrating a cross-section parallel to the normal direction $\mathbf{n}$ of the surface, where the three-dimensional body $\mathscr{D}_2$ with constant thickness $t_2$ is reduced to an equivalent material surface $\mathscr{S}$.

It is worth highlighting that the SSM framework is not limited to capturing only the membrane behavior of the coatings, as considered in this case, but is also capable of accounting for both in-plane and out-of-plane bending effects, which may be non-negligible for certain types of coatings.

## 3. Model validation

The proposed approach utilizes the Gurtin–Murdoch surface elasticity model to simulate the SFRM coatings applied to masonry walls.

A preliminary study is conducted on a sample system consisting of a $1 \times 1$ m masonry wall, coated on both sides with SFRM layers of thin thickness $t_c$ (see Fig. 3b). The masonry follows a running/header bond pattern (as depicted in Fig. 3a), with bricks of dimensions $a \times b \times t_b$, surrounded by mortar beds and joints of thickness $t_m$. The three basic components, namely brick, mortar, and SFRM coating, are assumed to be homogeneous and isotropic. Their respective Young modulus and Poisson ratio are denoted as $(E_b, \nu_b)$, $(E_m, \nu_m)$, and $(E_c, \nu_c)$. The elastic and geometric properties of each component, along with their mass densities ($\rho_b$, $\rho_m$, $\rho_c$), are detailed in Table 1. It is important to note that the equivalent properties of the SFRM coating are not derived from specific experimental tests. However, they are consistent with general experimental data available in the literature, such as those presented in Facconi et al. (2015). This approach reflects the objective of the study, which is not to investigate a particular type of SFRM — whose properties vary depending on the specific mixture used — but to assess the overall effects of this form of reinforcement on the masonry and validate the proposed model.

Three distinct FE models (Fig. 3) are implemented in COMSOL Multiphysics and described below:

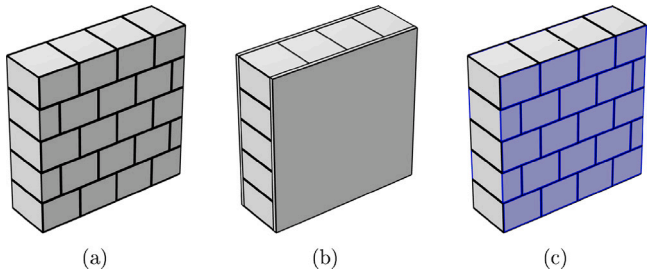


**Fig. 3.** FE models: (a) FM, (b) FMFC, (c) FMSC. (For interpretation of the references to color in this figure legend, the reader is referred to the web version of this article.)

**Table 1**
Elastic, geometric and mass characteristics of brick, mortar and SFRM coating.

| | |
|---|---|
| Brick | $E_b = 9$ GPa, $\nu_b = 0.15$<br>$a = 19$ cm, $b = 25$ cm, $t_b = 30$ cm<br>$\rho_b = 850$ kg/m$^3$ |
| Mortar | $E_m = 4$ GPa, $\nu_m = 0.2$<br>$t_m = 1$ cm<br>$\rho_m = 1400$ kg/m$^3$ |
| SFRM Coating | $E_c = 20$ GPa, $\nu_c = 0.18$<br>$t_c = 2.5$ cm<br>$\rho_c = 1800$ kg/m$^3$ |

(a) Fine Masonry (FM) model: Unreinforced masonry model, in which brick and mortar elements are finely modeled as Cauchy continuum bodies defined in a 3D space, each obeying to hyperelastic isotropic linear laws. Quadratic serendipity tetrahedral finite elements are used. Adherence conditions (i.e., no slip and no opening) are assured at the each element boundary. The model has 562,340 DOFs.

(b) Fine Masonry with Fine Coating (FMFC) model: Coated masonry model, in which brick, mortar and coating elements are finely modeled as Cauchy continuum bodies in a 3D space, each obeying to hyperelastic isotropic linear laws. Quadratic serendipity tetrahedral finite elements are used. Adherence conditions are assured at the each element boundary. The model has 625,070 DOFs, that is 11% more than FM model.

(c) Fine Masonry with Surface Stress Coating (FMSC) model: Coated masonry model, obtained by simply adding material surfaces (blue areas in Fig. 3c) to the FM model. This is accomplished by incorporating an additional surface weak form contribution, which is directly applied at the interfaces between the masonry and the coating. A more detailed explanation of the integration of the SSM into the FE framework can be found in Appendix A.1. The equivalent surface mass density and Lamé constants are $\rho_s = 45$ kg/m$^2$ and $\lambda_s = 1.19 \times 10^5$ kN/m, $\mu_s = 2.12 \times 10^5$ kN/m. It is important to emphasize that incorporating material surfaces into the FM model does not alter the system DOFs.

Static and dynamic (modal) numerical analyses are performed within the elastic regime using a linear solver. Each model is positioned in the $O(x, y, z)$ coordinate system, as shown in Fig. 4a. The main results focus on three key cutting lines, labeled as $H$, $V$, and $D$, which correspond to the Horizontal, Vertical, and Depth cutting lines, respectively, and are illustrated in Fig. 4b.

For clarity, it is important to mention that the results of the FM model, as defined here, will not be presented in this section, which is primarily focused on validating the SSM. Instead, the FM model is later employed in Section 4.1 to examine the impact of reinforcement on the structural behavior of the considered sample system, both in undamaged and damaged states.

### 3.1. Statics

Static analyses are first carried out by assuming the wall is constrained at the bottom, loaded on one face, and free on the remaining sides.

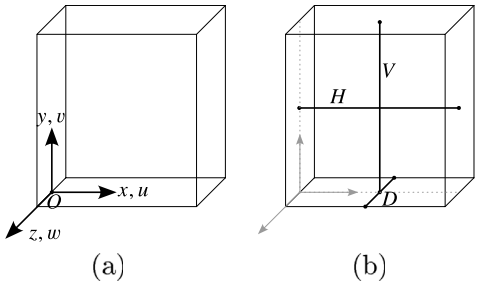


**Fig. 4.** (a) Coordinate system and displacement components; (b) cutting lines of interest.

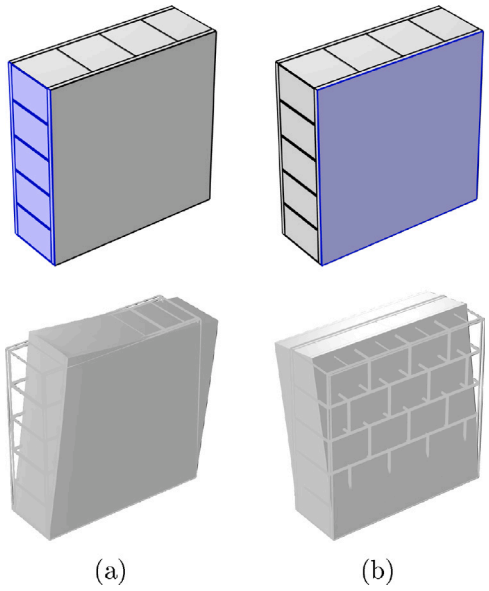


**Fig. 5.** (a) In-plane and (b) out-of-plane load conditions: loaded surfaces and deformed configurations. (For interpretation of the references to color in this figure legend, the reader is referred to the web version of this article.)

Two specific load conditions are considered: in-plane and out-of-plane. These are generated by applying a uniform normal pressure of $p_0 = 100$ kPa on the highlighted surfaces shown in Fig. 5a and b, respectively, along with their corresponding deformed configurations.

Numerical results are presented below, including displacements ($u$ and $w$) and stresses ($\sigma_x, \sigma_y, \tau_{xy}$ and $\sigma_z, \sigma_y, \tau_{yz}$) evaluated along the cutting lines in Fig. 4b. Displacements are measured in centimeters (cm), spatial coordinates in meters (m), and stresses in pascals (Pa).

Results for the FMFC (black line) and FMSC (red line) models are shown in Fig. 6 for the in-plane load case and in Fig. 7 for the out-of-plane load case. Comparisons are made in terms of both displacements and stresses. Strong agreement is observed in the in-plane case, with overlapping curves, whereas a slight discrepancy is noted in the out-of-plane response. This occurs because the addition of the SFRM layers generate an out-of-plane bending couple, driven by membrane stresses within the two coatings that are equal in magnitude but opposite in sign (as shown in Fig. 7c). When the coating is modeled as surface stress in the FMSC model, the couple arm decreases from $t_b + t_c$ to $t_b$, resulting in reduced stiffness, as reflected in the displacement curves in Fig. 7. This will also be confirmed by the dynamic analyses conducted later.

### 3.2. Free dynamics

Modal dynamic analyses are also conducted, assuming the walls are constrained at the bottom and free on the remaining sides.

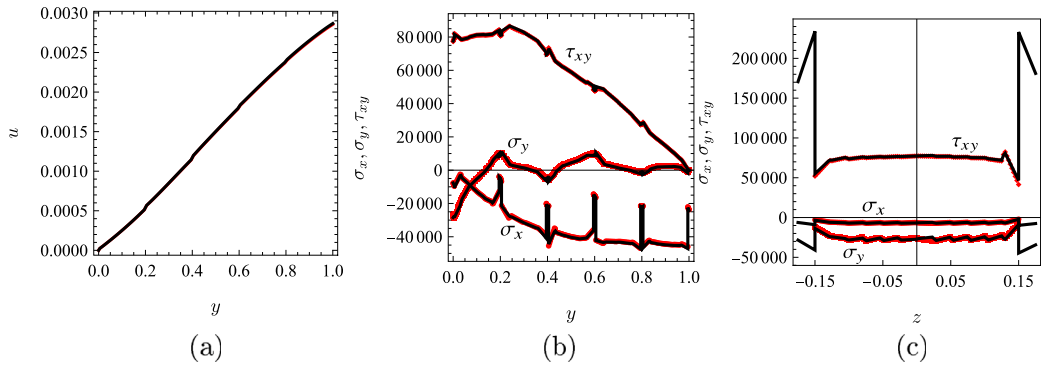


**Fig. 6.** Comparisons between FMFC (black line) and FMSC (red line) models under the in-plane load case: (a) displacements $u$ on cutting line $V$; stresses $\sigma_x, \sigma_y, \tau_{xy}$ on cutting lines (b) $V$ and (c) $D$. (For interpretation of the references to color in this figure legend, the reader is referred to the web version of this article.)

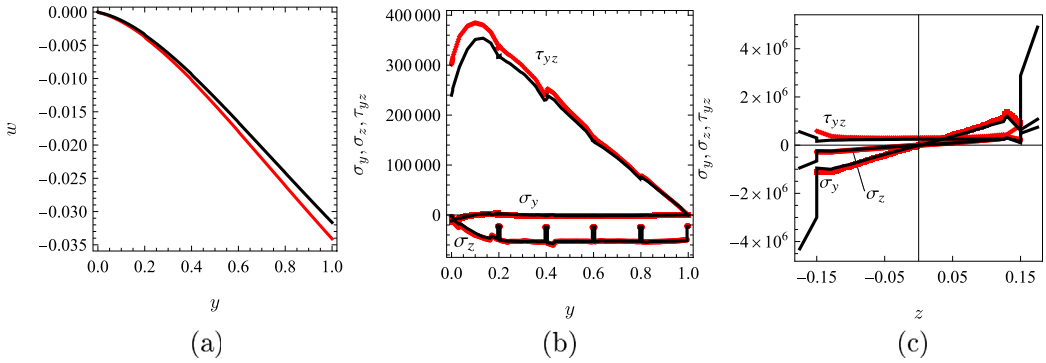


**Fig. 7.** Comparisons between FMFC (black line) and FMSC (red line) models under the out-of plane load case: (a) displacements $w$ on cutting line $V$; stresses $\sigma_y, \sigma_z, \tau_{yz}$ on cutting lines (b) $V$ and (c) $D$. (For interpretation of the references to color in this figure legend, the reader is referred to the web version of this article.)

**Table 2**
Comparisons between FMFC and FMSC models: natural frequencies (in [Hz]); percentage error $\epsilon$ in round brackets.

| Mode $n$ | Mode type | Modal frequency $f$ | |
|---|---|---|---|
| | | (FMFC) | (FMSC) |
| 1 | I out-of-plane | 180.40 | 173.94 (−3.58%) |
| 2 | I in-plane | 333.46 | 334.33 (0.26%) |
| 3 | II out-of-plane | 359.70 | 344.87 (−4.12%) |
| 4 | III out-of-plane | 767.87 | 737.93 (−3.9%) |
| 5 | II in-plane | 783.38 | 787.15 (0.48%) |
| 6 | III in-plane | 900.03 | 902.48 (0.27%) |

The results include the frequencies $f$ of the first six natural vibration modes ($n = 1, \dots, 6$), with their modal shapes shown in Fig. 8. Comparisons between the FMFC and FMSC models are presented in Table 2, where a relative percentage error, defined as $\epsilon := \frac{f^{FMSC} - f^{FMFC}}{f^{FMFC}}$, is included in round bracket. The results demonstrate strong agreement, although larger (yet still acceptable) errors are observed for the out-of-plane modes, consistent with findings from static analyses and subject to further confirmation.

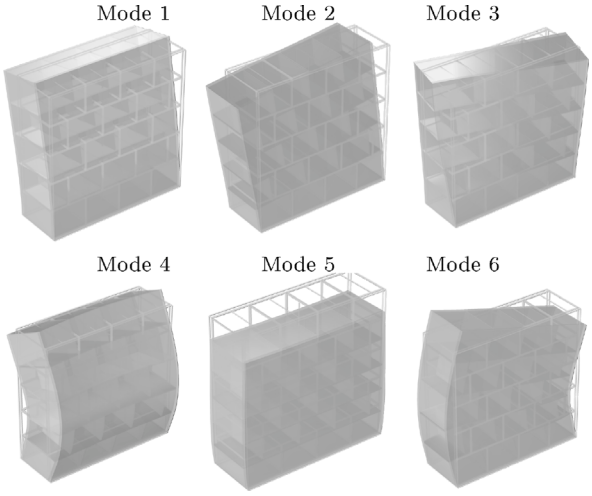


**Fig. 8.** Modal shapes of the FMFC model.

## 4. Numerical application

### 4.1. Discussion on the influence of the reinforcement

This section explores the effect of the coating when applied to: (i) entire facades of intact masonry walls to enhance their performance, and (ii) damaged areas of masonry walls to restore them to their original condition.

#### 4.1.1. Fully coated masonry

Parametric analyses are performed on the FM, FMFC, and FMSC models described in Section 3 to investigate the influence of both the modulus $E_c$ and thickness $t_c$ of the SFRM coating on the system modal dynamics. To this end, the non-dimensional ratios $\alpha = \frac{E_c}{E_b}$ and $\beta = \frac{t_c}{t_b}$ are introduced, along with the parameter $\eta := \frac{f}{f^{FM}}$, which represents the frequency ratio relative to the unreinforced model.

The results of the FMFC (black line) and FMSC (red line) models are compared in terms of the frequencies of both the first out-of-plane and first in-plane modes, shown respectively in Figs. 9 and 10. The absolute value of the relative percentage error $|\epsilon|$ is also calculated.

Firstly, with respect to the accuracy of the FMSC model, the results from Section 3 are confirmed: the model yields higher accuracy for

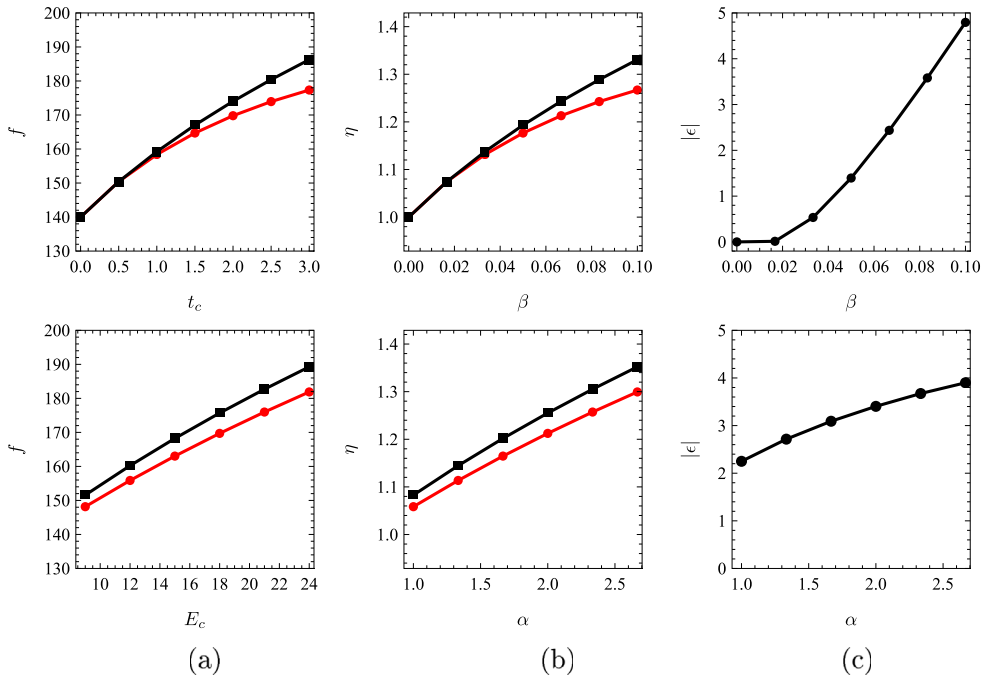


**Fig. 9.** Parametric analysis of the first out-of-plane natural mode (Fig. 8a). Comparison between FMFC (black line) and FMSC (red line) models: (a) frequency, (b) frequency ratio $\eta$ and (c) relative percentage error $|\epsilon|$. (For interpretation of the references to color in this figure legend, the reader is referred to the web version of this article.)

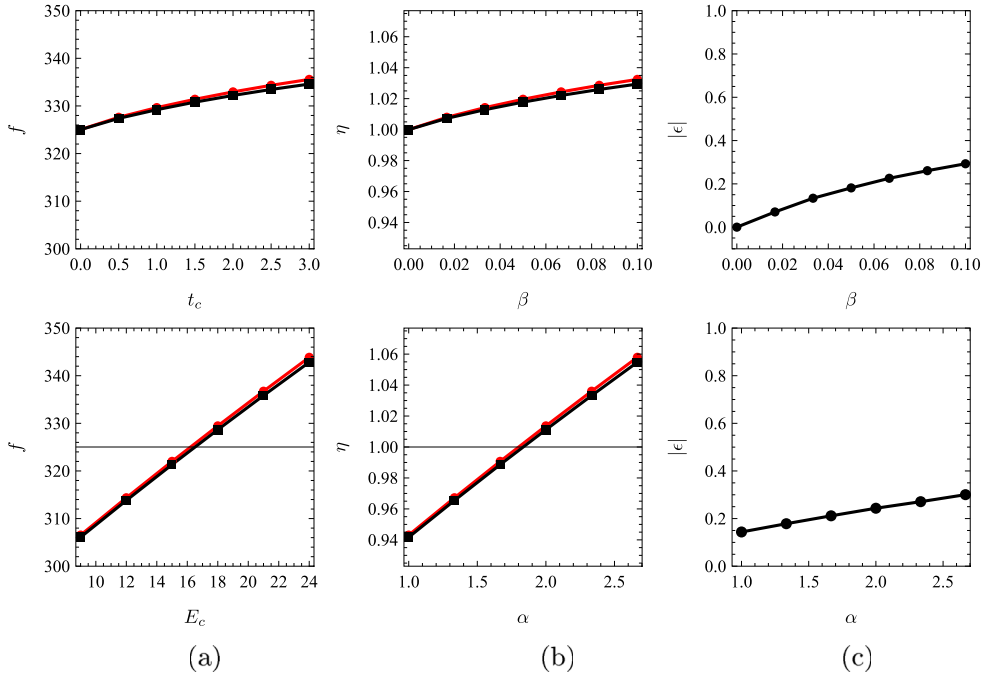


**Fig. 10.** Parametric analysis of the first in-plane natural mode (Fig. 8b). Comparison between FMFC (black line) and FMSC (red line) models: (a) frequency, (b) frequency ratio $\eta$ and (c) relative percentage error $|\epsilon|$. (For interpretation of the references to color in this figure legend, the reader is referred to the web version of this article.)

the in-plane mode, with a maximum error of approximately 0.3%, compared to the out-of-plane mode, where the maximum error is around 5%.

Regarding the impact of reinforcement, the addition of coating layers affects out-of-plane and in-plane vibration modes differently. The coating increases wall stiffness, generally resulting in higher frequencies compared to the unreinforced walls (i.e., the FM model). This behavior is consistent with the trend of the parameter $\eta$ related to the first out-of-plane mode, as shown in Fig. 9b. However, this effect is not always observed in the in-plane mode, where for certain values of the SFRM elastic modulus, $\eta < 1$, as illustrated in Fig. 10b. This occurs mainly because the coating adds mass to the wall, which can, in some cases, counteract the benefits of increased stiffness, thus inhibiting the anticipated rise in natural frequencies. Finally, within the examined ranges, it is seen that reinforcement can increase the natural frequency of the first out-of-plane mode by up to 30%, whereas its effect on the first in-plane mode frequency is considerably smaller. As a result, for sufficiently large values of $t_c$ and $E_c$, the coating causes an inversion of the second (II out-of-plane) and third (I in-plane) modes.

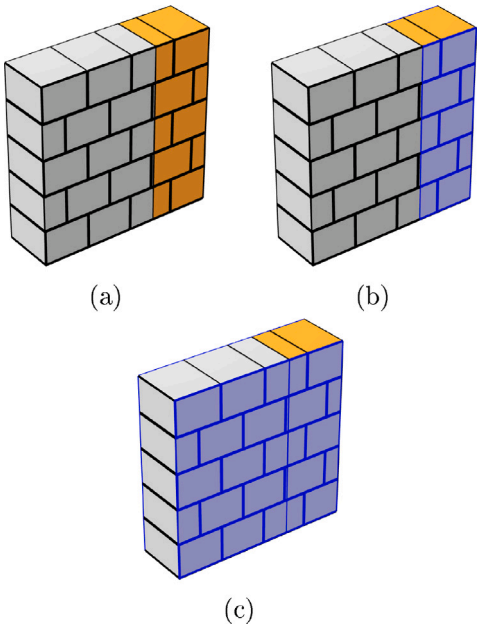


**Fig. 11.** FE models: (a) FDM, (b) FDMSC-p, (c) FDMSC-f. (For interpretation of the references to color in this figure legend, the reader is referred to the web version of this article.)

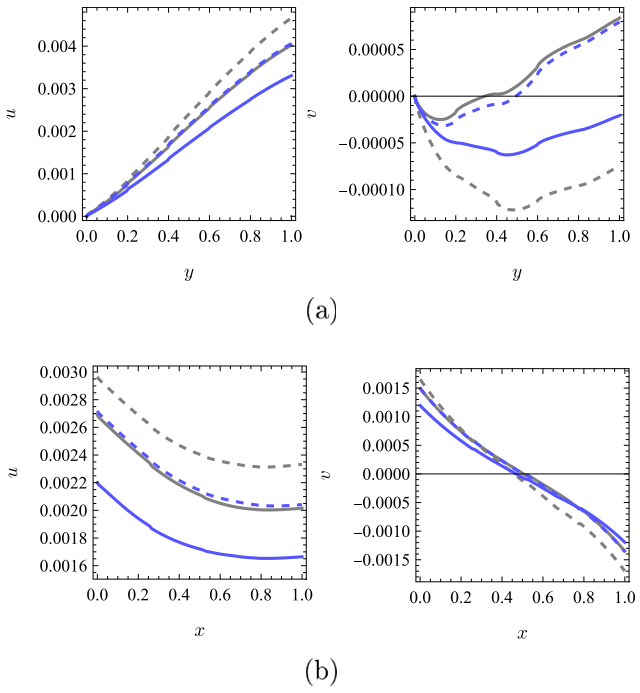


**Fig. 12.** Displacements $u$ and $v$ along the cutting line: (a) $V$; (b) $H$. Comparisons among FM (gray solid line), FDM (gray dashed line), FDMSC-p (blue dashed line) and FDMSC-f (blue solid line) models. (For interpretation of the references to color in this figure legend, the reader is referred to the web version of this article.)

#### 4.1.2. Partially/fully coated damaged masonry

A portion of the masonry wall is now considered damaged. This damaged area is assumed to be a vertical strip with a width of 1/3 m, as shown in orange in Fig. 11a. Two types of repairs are examined using coatings: (i) partial, where the SFRM layers are applied only in the vicinity of the damaged area (blue surfaces in Fig. 11b); and (ii) full, where the SFRM layers are applied across the entire wall facades (blue surfaces in Fig. 11c).

To this aim, three new FE models are implemented (Fig. 11):

- Fine Damaged Masonry (FDM) model: unreinforced and damaged masonry model, derived from the FM model by reducing the elastic moduli of the damaged elements. Specifically, the elastic moduli for the damaged mortar and brick are assumed to be $\frac{2}{3}E_m$ and $\frac{2}{3}E_b$, respectively.
- Fine Damaged Masonry with Surface Stress Coating - partial (FDMSC-p) model: damaged masonry model, partially reinforced near the damaged areas. It is derived from the FDM model by adding material surfaces (highlighted in blue in Fig. 11b). In these areas, surface stress boundary conditions, as described by Eq. (A.10), are applied.
- Fine Damaged Masonry with Surface Stress Coating - full (FDMSC-f) model: damaged masonry model, fully reinforced. It is derived from the FDM model by adding material surfaces across the entire wall facades (blue areas in Fig. 11c). Surface stress boundary conditions, similar to the previous ones, are applied to these areas.

Static analyses are conducted in the elastic regime on the previously described FE models, all of which maintain the same DOFs as the FM model. The wall is subjected to the same in-plane load condition as outlined in Section 3.1 and illustrated in Fig. 5a.

The relevant results are shown in Fig. 12, where the displacements of the FM (solid gray line), FDM (dashed gray line), FDMSC-p (dashed blue line), and FDMSC-f (solid blue line) models are compared. It is observed that the FDM model exhibits larger displacements than the FM model, indicating that even partial damage significantly reduces the system stiffness. However, the application of partial SFRM coating (FDMSC-p model) results in a recovery of stiffness, bringing the performance back to the initial conditions. Moreover, reinforcing the entire wall (FDMSC-f model) not only restores but also improves performance beyond the undamaged state.

### 4.2. Application to a "real" case

Finally, the SSM is used to simulate the SFRM coatings applied to a structural system, consisting of a two-story masonry wall with four openings; its in-plane geometry is depicted in Fig. 13, where the dimensions are expressed in meters.

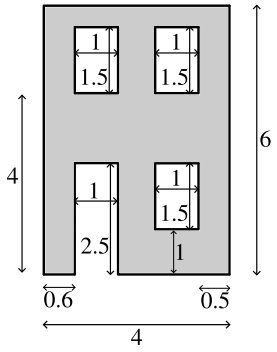


**Fig. 13.** In-plane geometry of the structural masonry sample.

Below, the impact of partial and full coatings is investigated, addressing both intact and damaged conditions of the masonry. Additionally, the accuracy of the SSM and its benefits in computational performance are demonstrated.

#### 4.2.1. Fully coated structural masonry

The masonry wall, featuring the same running/header bond pattern described in Section 3, is fully coated on both sides with thin layers of

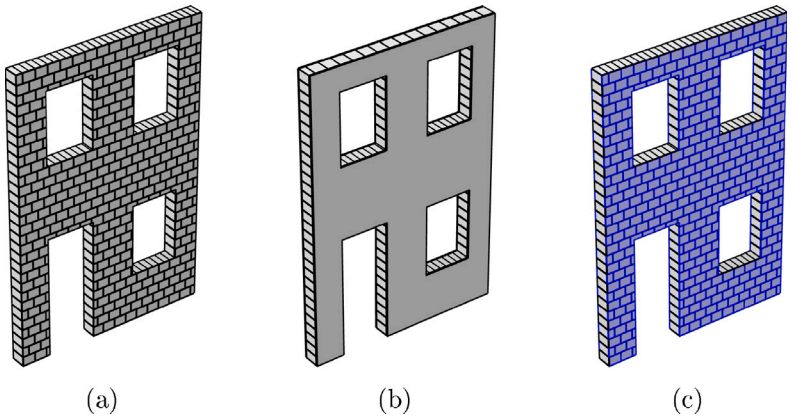


**Fig. 14.** FE models of the structural masonry sample: (a) FM, (b) FMFC, (c) FMSC. (For interpretation of the references to color in this figure legend, the reader is referred to the web version of this article.)

**Table 3**
Natural frequencies $f^{FM}$ (in [Hz]) of FM structural model.

| Mode | Mode type | Modal frequency |
|---|---|---|
| 1 | I out-of-plane | 24.729 |
| 2 | I in-plane | 28.584 |
| 3 | II out-of-plane | 44.457 |

SFRM, as shown in Fig. 3b. The elastic, geometric and mass properties of the basic elements are detailed in the previous Table 1.

To further assess the performance of the SSM and evaluate the effectiveness of the reinforcement, the following three FE models are defined (see Fig. 14):

- Fine Masonry (FM) structural model: Unreinforced structural masonry model, where masonry elements are finely modeled as Cauchy continuum bodies in 3D space, each following hyperelastic isotropic linear laws. Quadratic serendipity tetrahedral finite elements are used, with adherence conditions maintained at each element boundary. The model has 2,201,136 DOFs.
- Fine Masonry with Fine Coating (FMFC) structural model: Coated structural masonry model, in which brick, mortar and coating elements are finely modeled as Cauchy continuum bodies in a 3D space, each following hyperelastic isotropic linear laws. Quadratic serendipity tetrahedral finite elements are used, with adherence conditions at each element boundary. The model has 3,035,138 DOFs, that is 37.9% more than the FM structural model.
- Fine Masonry with Surface Stress Coating (FMSC) structural model: Coated structural masonry model, which is defined by adding material surfaces across the entire wall facades of the FM structural model. Surface stress boundary conditions, as specified in Eq. (A.10), are applied to the blue areas highlighted in Fig. 14c. The model retains the same DOFs as the FM structural model.

Dynamic modal analyses are conducted for each of the aforementioned models using commercial software and a linear solver. The walls are clamped at the bottom and hinged along the vertical sides. The results include the modal frequencies $f$ and the corresponding modal shapes for the first three natural vibration modes.

First, the modal frequencies $f^{FM}$ of the FM structural model, along with their corresponding modal shapes, are reported in Table 3 and Fig. 15, respectively. The calculation time was of 214 s (i.e., 3 min, 34 s).

Next, the natural frequencies of the FMFC ($f^{FMFC}$) and FMSC ($f^{FMSC}$) structural models are evaluated and compared. Specifically, the $f^{FMSC}$ values are reported in Table 4, along with the percentage error $\epsilon$ (defined as $\epsilon := \frac{f^{FMSC}-f^{FMFC}}{f^{FMFC}}$) in brackets. Additionally, the effect of reinforcement is assessed by evaluating the frequency ratio $\eta := \frac{f^{FMSC}}{f^{FM}}$. While the solution time for the FMSC structural model was the same as that of the FM one, the calculation time for the FMFC structural model was 1308 s (i.e., 21 min and 48 s), which is six times longer.

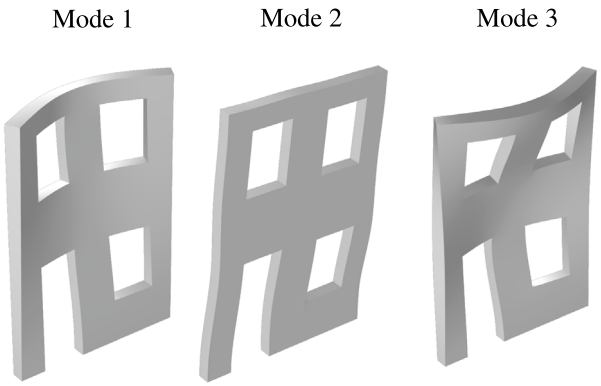


**Fig. 15.** Modal shapes of the FM structural model.

**Table 4**
Natural frequency $f^{FMSC}$ (in [Hz]) of FMSC structural model; percentage error $\epsilon$ in round brackets and frequency ratio $\eta$.

| Mode | Mode type | Modal frequency | $\eta$ |
|---|---|---|---|
| 1 | I in-plane | 29.440 (0.44%) | 1.025 |
| 2 | I out-of-plane | 31.335 (−3.61%) | 1.315 |
| 3 | II out-of-plane | 55.230 (−3.56%) | 1.289 |

The results confirm the accuracy of the SSM and the effectiveness of the coating. The FMSC structural model demonstrates high accuracy, with a slightly greater approximation in the out-of-plane modes. The primary effect of the coating is to increase the natural frequency of the out-of-plane modes by 30%, while its impact on the in-plane modes is less pronounced. Consequently, a mode inversion occurs between the first (I out-of-plane) and second (I in-plane) modes. A notable advantage is the significant computational time savings achieved due to the lower number of DOFs in the FMSC structural model compared to the FMFC one.

#### 4.2.2. *Fully/partially coated structural damaged masonry*

The structural masonry sample is now assumed to be partially damaged, as indicated by the damage map (orange areas) shown in Fig. 16a. This map is derived from the stress distribution observed in the first in-plane natural mode (Fig. 15b), considering a typical in-plane failure mechanism. Two repair strategies are proposed: (i) partial application of SFRM coatings to the facades of the first story only

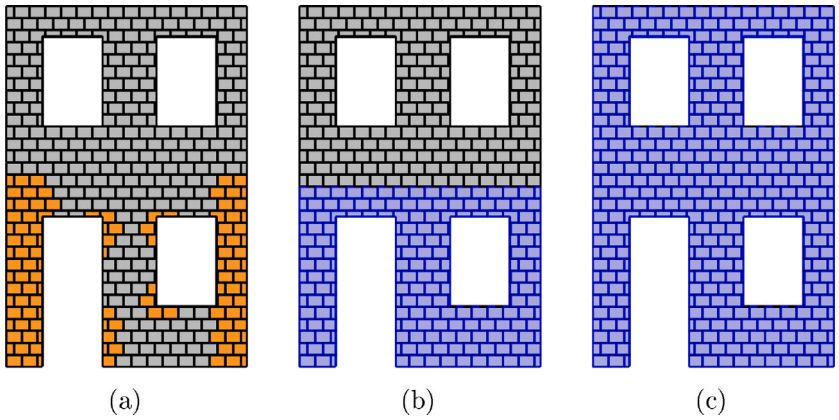


**Fig. 16.** FE models of the structural masonry sample: (a) FDM, (b) FDMSC-p, (c) FDMSC-f. (For interpretation of the references to color in this figure legend, the reader is referred to the web version of this article.)

**Table 5**
Natural frequencies of the FDM structural model (in [Hz]) and frequency ratio $\delta$.

| Mode | Mode type | Modal frequency | $\delta$ |
|---|---|---|---|
| 1 | I out-of-plane | 24.196 | 0.978 |
| 2 | I in-plane | 24.952 | 0.873 |
| 3 | II out-of-plane | 43.148 | 0.970 |

**Table 6**
Frequency ratio relative to the FDM structural model, $\delta_c$, for the FDMSC-p and FDMSC-f structural models.

| Mode | FDMSC-p | | FDMSC-f | |
|---|---|---|---|---|
| | Mode type | $\delta_c$ | Mode type | $\delta_c$ |
| 1 | I out-of-plane | 1.06 | I in-plane | 0.94 |
| 2 | I in-plane | 1.04 | I out-of-plane | 1.25 |
| 3 | II out-of-plane | 1.06 | II out-of-plane | 1.22 |

(highlighted in blue in Fig. 16b); and (ii) full application of SFRM coatings to the entire facade (Fig. 16c).

Three FE models are implemented (see Fig. 16):

- Fine Damaged Masonry (FDM) structural model: unreinforced and damaged masonry structural model, derived from the FM structural model by reducing the elastic moduli of the damaged elements. Specifically, the elastic moduli for the damaged mortar and brick are assumed to be $\frac{2}{3}E_m$ and $\frac{2}{3}E_b$, respectively.
- Fine Damaged Masonry with Surface Stress Coating - partially (FDMSC-p) structural model: damaged masonry structural model, partially reinforced near the damaged areas. It is derived from the FDM structural model by adding material surfaces to the facades of the first story. In these areas, surface stress boundary conditions, as described by Eq. (A.10), are applied.
- Fine Damaged Masonry with Surface Stress Coating - fully (FDMSC-f) structural model: damaged masonry structural model, fully reinforced. It is derived from the FDM model by adding material surfaces across the entire wall facades. Surface stress boundary conditions are applied to these areas.

Dynamic modal analyses are conducted in the elastic regime on the previously described FE models, all of which maintain the same DOFs as the FM structural model. The natural frequencies and corresponding modal shapes for the first three vibration modes are evaluated.

First, the frequencies of the FDM structural model, $f^{FDM}$, are presented in 5. To assess the impact of the damage, the frequency ratio relative to the FM structural model is evaluated as $\delta := \frac{f^{FDM}}{f^{FM}}$. As expected, the damage leads to a significant reduction in system stiffness for the first in-plane mode (Mode 2), causing a frequency decrease of approximately 13%. In contrast, the frequencies of the other modes remain largely unchanged.

Next, the natural frequencies of the FDMSC-p ($f^{FDMSC-p}$) and FDMSC-f ($f^{FDMSC-f}$) structural models are evaluated and compared with the previous ones. Especially, the effect of reinforcement is assessed by evaluating the frequency ratio $\delta_c := \frac{f^{FDMSC}}{f^{FM}}$, reported in Table 6.

It is observed that the partial application of SFRM coatings (in the FDMSC-p structural model) leads to a significant recovery of the dynamic properties, effectively restoring the system performance to its initial state. Notably, in the first in-plane mode (Mode 2), the frequency ratio $\delta_c = 1.0607$, compared to $\delta = 0.872936$, shows a 16% increase in frequency. On the other hand, the full application of SFRM coatings (in the FDMSC-f structural model) produces distinct effects, with the most prominent being an improvement in the out-of-plane response. Specifically, the frequency ratios $\delta_c \approx 1.2$ in both Modes 2 and 3 (compared with $\delta \approx 0.97$) indicate a frequency increase of about 25%. However, the in-plane dynamic characteristics are not fully restored, as seen in Mode 1, where $\delta_c = 0.941226$. This is because the increase in stiffness is not sufficient to compensate for the additional mass introduced by the coating. Consequently, an inversion occurs between the first (out-of-plane) and second (in-plane) natural modes.

## 5. Conclusions and future purposes

The in-plane and out-of-plane behavior of masonry structures reinforced with thin coatings, such as Steel Fiber Reinforced Mortar (SFRM), has been studied using the Surface Stress Model (SSM). This approach involves: (i) detailed three-dimensional finite element models for unreinforced masonry, and (ii) the application of the SSM for the coatings. Notably, this marks the first use of the Gurtin–Murdoch SSM in the analysis of masonry buildings. FE analyses have been performed within the elastic regime on coated masonry walls, under both static and dynamic conditions. Both intact and damaged masonry walls have been investigated.

The key findings are outlined below:

- This study demonstrates the effectiveness of the Gurtin-Murdoch Surface Stress Model (SSM) in accurately capturing the surface stress effects of thin coatings used in masonry reinforcement. Originally developed within the field of nanomechanics, the SSM has shown strong potential for application in large-scale civil engineering problems, offering a computationally efficient alternative to conventional finite element (FE) modeling approaches. The latter require the explicit modeling of additional elements, interface conditions, and specialized meshing strategies to represent

thin coatings—factors that increase both complexity and computational cost. In contrast, the proposed SSM approach avoids the need to define new elements and preserves the original degrees of freedom of the model, thereby significantly reducing computational effort without compromising accuracy. The results confirm that the SSM is a practical and efficient tool for evaluating reinforcement strategies, as it can be seamlessly integrated into existing FE models without requiring complex remeshing or the development of entirely new models.

- The numerical results show that the application of SFRM coatings increases the stiffness of masonry walls, generally raising their natural frequencies. Beyond enhancing overall wall performance, SFRM can also be used to repair damaged sections, effectively restoring the wall to its original condition. Additionally, this reinforcement has been found to affect out-of-plane and in-plane wall behavior differently, with the most significant impact observed in out-of-plane behavior due to bending couples generated by membrane stresses in the coatings. This can potentially lead to an inversion of the natural modes.

This work represents a step forward in leveraging SSM for evaluating the effects of reinforcement coatings in masonry structures, highlighting its potential benefits for integration into widely used engineering tools. Several promising directions for future development can be explored. Some are listed below:

- Extending SSM to nonlinear analyses – Future developments will aim to extend the SSM framework to account for nonlinear behavior, thereby increasing its applicability to real-world structures under extreme loading conditions. A natural first step could involve the adoption of damage-based constitutive laws for the masonry (e.g., Di Nino et al., 2017), while preserving the elastic behavior of the coating. This modeling choice is supported by experimental evidence (e.g., Facconi et al., 2015) that show widespread cracking in the masonry rather than in the coating. Moreover, nonlinear formulations of the SSM, such as those based on finite elasticity (e.g., Steigmann and Ogden, 1999), are already available in the literature and could be integrated into the current framework. Another promising direction involves the incorporation of delamination phenomena, which represent a potential critical failure mode in coated masonry systems. Thanks to its flexibility, the SSM framework can be extended to account for interfacial failure mechanisms. By embedding cohesive or softening constitutive laws into the surface formulation, the SSM can effectively simulate the progressive loss of adhesion at the interface, thereby capturing delamination behavior.
- Application to other reinforcement techniques – The framework will be extended to include additional reinforcement strategies by leveraging the flexibility of the SSM approach, which is capable of supporting the implementation of a wide range of constitutive laws, including custom or non-standard models. This enables the modeling of various thin reinforcement systems. In particular, a first extension will target thin coatings exhibiting an in-plane orthotropic behavior (such as Fiber-Reinforced Polymers), which can be incorporated by appropriately modifying the constitutive laws in the second of Eq. (2) (or in the first of Eq. (A.4)).
- Integration into commercial software – While COMSOL Multiphysics provides the flexibility needed to implement the proposed Surface Stress Model (SSM), extending the approach to other widely used commercial platforms presents nontrivial challenges. It would require the development of custom material subroutines or user-defined elements, depending on the architecture and capabilities of each software environment. Future work could focus on integrating the SSM into commonly used structural analysis tools, thereby promoting its adoption in practical engineering applications for both design and assessment.
- Investigation of complex geometries – The model will be applied to structures with intricate geometries, such as historical buildings and monuments, to evaluate its effectiveness in real-world scenarios.

## CRediT authorship contribution statement

**Simona Di Nino:** Writing – review & editing, Writing – original draft, Visualization, Validation, Software, Methodology, Investigation, Formal analysis. **Giuseppe Rosi:** Writing – review & editing, Methodology, Conceptualization. **Francesco D'Annibale:** Writing – review & editing, Validation, Supervision, Conceptualization.

## Declaration of competing interest

The authors declare that they have no known competing financial interests or personal relationships that could have appeared to influence the work reported in this paper.

## Appendix. Variational approach of the SSM

The Hamilton variational principle is employed for the SSM by defining the action functional (Hamiltonian) over a specified time interval $[t_1, t_2]$ as follows:

$$\mathcal{H} := \int_{t_1}^{t_2} (K - \Pi)\, dt, \tag{A.1}$$

where $\Pi$ is the total potential energy and $K$ denotes the kinetic energy. These are defined as follows:

$$\begin{aligned} \Pi &:= \int_{\mathscr{D}_1} \mathcal{U}\, dV + \int_{\mathscr{S}} \mathcal{U}_s\, dS - \int_{\partial\mathscr{D}_f} \mathbf{f}^T \mathbf{u}\, dS, \\ K &:= \int_{\mathscr{D}_1} \mathcal{K}\, dV + \int_{\mathscr{S}} \mathcal{K}_s\, dS. \end{aligned} \tag{A.2}$$

whose domain encompasses the space of kinematically admissible functions $\mathbf{u}$, such that $\mathbf{u} = \bar{\mathbf{u}}$ on $\partial\mathscr{D}_u$. Here, $\mathcal{U}, \mathcal{K}$ and $\mathcal{U}_s, \mathcal{K}_s$ represent the strain and kinetic energy densities of the body $\mathscr{D}_1$ and the material surface $\mathscr{S}$, respectively. They are written as:

$$\begin{aligned} \mathcal{U} &= \frac{1}{2}\left(\lambda_1 \mathrm{tr}\,(\mathbf{E})^2 + 2\mu_1 \mathrm{tr}\left(\mathbf{E}^2\right)\right), \\ \mathcal{K} &= \frac{1}{2}\rho_1 \dot{\mathbf{u}}^T \dot{\mathbf{u}}, \end{aligned} \quad \text{in } \mathscr{D}_1, \tag{A.3}$$

and:

$$\begin{aligned} \mathcal{U}_s &= \frac{1}{2}\left(\lambda_s \mathrm{tr}\left(\mathbf{E}_s\right)^2 + 2\mu_s \mathrm{tr}\left(\mathbf{E}_s^2\right)\right), \\ \mathcal{K}_s &= \frac{1}{2}\rho_s \dot{\mathbf{u}}^T \dot{\mathbf{u}}, \end{aligned} \quad \text{in } \mathscr{S}. \tag{A.4}$$

Finally, the variational equation $\delta\mathcal{H} = 0$ results in the following:

$$\begin{aligned} &\left(\int_{\mathscr{D}_1} \delta\mathcal{K} dV - \int_{\mathscr{D}_1} \delta\mathcal{U} dV\right) + \left(\int_{\mathscr{S}} \delta\mathcal{K}_s dS - \int_{\mathscr{S}} \delta\mathcal{U}_s dS\right) \\ &\qquad + \int_{\partial\mathscr{D}_f +} \mathbf{f}^T \delta\mathbf{u} dS = 0, \end{aligned} \tag{A.5}$$

where:

$$\begin{aligned} \delta\mathcal{K} &= \rho_1 \dot{\mathbf{u}}^T \delta\dot{\mathbf{u}}, \\ \delta\mathcal{U} &= \lambda_1 \mathrm{tr}\,(\mathbf{E})\,\mathrm{tr}\,(\delta\mathbf{E}) + 2\mu_1 \mathrm{tr}\,(\mathbf{E}\delta\mathbf{E}), \end{aligned} \quad \text{in } \mathscr{D}_1 \tag{A.6}$$

and:

$$\begin{aligned} \delta\mathcal{K}_s &= \rho_s \dot{\mathbf{u}}^T \delta\dot{\mathbf{u}}, \\ \delta\mathcal{U}_s &= \lambda_s \mathrm{tr}\left(\mathbf{E}_s\right)\mathrm{tr}\left(\delta\mathbf{E}_s\right) + 2\mu_s \mathrm{tr}\left(\mathbf{E}_s \delta\mathbf{E}_s\right), \end{aligned} \quad \text{in } \mathscr{S}. \tag{A.7}$$

Eq. (A.5) holds for every kinematically admissible $\mathbf{u}$ and $\delta\mathbf{u}$, representing the elastic problem in its weak form. It can be demonstrated that the strong form of the elastic problem, as presented in Section 2.1, can be derived from Eq. (A.5). For further details, please refer to Gurtin and Ian Murdoch (1975).

### A.1. Application of the SSM to the sample system

The previous variational formulation of the Gurtin-Murdoch model, expressed through the variational equations Eq. (A.7), is now specialized to the sample system described in Section 3. This is done with the aim of implementing the SSM within the FE framework, as will be clarified later. Accordingly, the material surfaces $\mathscr{S}$ coincide with masonry-coating interfaces, highlighted by the blue areas in Fig. 3c. The outward unit normal to $\mathscr{S}$ is given by $\mathbf{n} = \begin{Bmatrix} 0 & 0 & \pm 1 \end{Bmatrix}^T$, depending on the facade under consideration. In what follows, the focus is on the surface where $\mathbf{n} = \begin{Bmatrix} 0 & 0 & 1 \end{Bmatrix}^T$, for which the projection tensor Eq. (3) is:

$$\mathbf{P} = \begin{bmatrix} 1 & 0 & 0 \\ 0 & 1 & 0 \\ 0 & 0 & 0 \end{bmatrix}. \tag{A.8}$$

Thus, being $\mathbf{u} = \begin{Bmatrix} u & v & w \end{Bmatrix}^T$ the displacement vector (Fig. 4a), the surface strain tensor Eq. (2)c reads:

$$\mathbf{E}_s = \begin{bmatrix} u_x & \frac{1}{2}\left(u_y + v_x\right) & 0 \\ \frac{1}{2}\left(u_y + v_x\right) & v_y & 0 \\ 0 & 0 & 0 \end{bmatrix}. \tag{A.9}$$

Finally, substituting into Eq. (A.7), the variations of the surface strain and kinetic energy densities are obtained as:

$$\begin{aligned} \delta\mathcal{K}_s =& \rho_s \left(\delta\dot{u}\,\dot{u} + \delta\dot{v}\,\dot{v} + \delta\dot{w}\,\dot{w}\right), \\ \delta\mathcal{U}_s =& \lambda_s(\delta u_x + \delta v_y)\left(u_x + v_y\right) + \mu_s \left(2\delta u_x u_x + 2\delta v_y v_y \right. \\ & \left. \left(\delta u_y + \delta v_x\right)\left(u_y + v_x\right)\right). \end{aligned} \tag{A.10}$$

In this context, the equivalent surface mass density and Lamé constants are derived from Eq. (5); therefore, with $\mathscr{D}_2$ representing the SFRM coatings, the relations $\rho_s = \rho_c t_c$, $\lambda_s = \lambda_c t_c$ and $\mu_s = \mu_c t_c$ are obtained.

*Implementation of the SSM in FE models*

The implementation of the SSM in the FE framework is carried out using the Weak Form PDE module in COMSOL Multiphysics. In this approach, the surface stress is applied following the variational formulation of the Gurtin-Murdoch model. Unlike conventional methods that introduce the SSM as a standard membrane element, this implementation includes an additional surface weak form contribution, directly applied on the surfaces of the masonry wall.

Specifically, the approach involves assigning the variations in surface energy density — both elastic and kinetic — as derived from Eq. (A.10), to the masonry-coating interfaces. These variations are incorporated into the weak form of the governing equations, allowing surface stress effects to be included without the need to explicitly model the coating as a separate structural element. Practically, the implementation follows two steps:

- Definition of coating interfaces: The surfaces representing the interface between the masonry and the coating are selected within the FE model.
- Application of surface energy variations: Using the Weak Form PDE module, the expressions for the energy variations (Eq. (A.10)) are assigned directly to these surfaces as source terms in the energy balance.

This approach enables the inclusion of surface stress effects in a consistent and efficient manner, preserving the accuracy of the model without complicating the numerical discretization. It is evident that one key advantage of this method is its ability to quickly incorporate reinforcement layers directly into existing FE models by simply selecting the reinforced surface, eliminating the need to create new models.

## Data availability

No data was used for the research described in the article.

## References


Addessi, D., Sacco, E., Paolone, A., 2010. Cosserat model for periodic masonry deduced by nonlinear homogenization. Eur. J. Mech. A Solids 29 (4), 724–737.

Adhikary, D.P., Dyskin, A.V., 1997. A Cosserat continuum model for layered materials. Comput. Geotech. 20 (1), 15–45.

Altenbach, H., Eremeev, V.A., Morozov, N.F., 2010. On equations of the linear theory of shells with surface stresses taken into account. Mech. Solids 45, 331–342.

Altenbach, H., Eremeyev, V.A., 2011. On the shell theory on the nanoscale with surface stresses. Internat. J. Engrg. Sci. 49 (12), 1294–1301.

Altenbach, H., Eremeyev, V.A, Morozov, N.F., 2012. Surface viscoelasticity and effective properties of thin-walled structures at the nanoscale. Internat. J. Engrg. Sci. 59, 83–89.

Angiolilli, M., Gregori, A., Pathirage, M., Cusatis, G., 2020. Fiber reinforced cementitious matrix (FRCM) for strengthening historical stone masonry structures: Experiments and computations. Eng. Struct. 224, 111102.

Bhattacharya, S., Nayak, S., Dutta, S.C., 2014. A critical review of retrofitting methods for unreinforced masonry structures. Int. J. Disaster Risk Reduct. 7, 51–67.

Biot, M.A., 1967. Rheological stability with couple stresses and its application to geological folding. Proc. R. Soc. Lond. Ser. A. Math. Phys. Sci. 298 (1455), 402–423.

Buyukkaragoz, A., Kopraman, Y., 2021. In-plane behaviour of masonry brick walls strengthened with mortar from two sides. In: Structures. Vol. 29, Elsevier, pp. 1627–1639.

Como, M., 2013. Statics of Historic Masonry Constructions. Vol. 1, Springer.

Dahmen, K., Lehwald, S., Ibach, H., 2000. Bending of crystalline plates under the influence of surface stress–a finite element analysis. Surf. Sci. 446 (1–2), 161–173.

Di Nino, S., 2022. Numerical investigations on infilled frames and predictive formulae in the elastic regime. Eng. Struct. 250, 113349.

Di Nino, S., D'Annibale, F., Luongo, A., 2017. A simple model for damage analysis of a frame-masonry shear-wall system. Int. J. Solids Struct. 129, 119–134.

Di Nino, S., Luongo, A., 2019. A simple homogenized orthotropic model for in-plane analysis of regular masonry walls. Int. J. Solids Struct. 167, 156–169.

Di Nino, S., Luongo, A., 2023. Two-step homogenized elastic model for in-plane analysis of coated masonry walls. Eur. J. Mech. A Solids 102, 105107.

Di Nino, S., Luongo, A., 2024. In-plane structural analysis of coated masonry walls via a homogenized model. Appl. Sci. 14 (3), 1091.

Di Nino, S., Zulli, D., 2020. Homogenization of ancient masonry buildings: A case study. Appl. Sci. 10 (19), 6687.

Eltaher, M.A., Mahmoud, F.F., Assie, A.E., Meletis, E.I., 2013. Coupling effects of nonlocal and surface energy on vibration analysis of nanobeams. Appl. Math. Comput. 224, 760–774.

Eremeyev, V.A., 2024. Surface finite viscoelasticity and surface anti-plane waves. Internat. J. Engrg. Sci. 196, 104029.

Eremeyev, V.A., Altenbach, H., Morozov, N.F., 2009. The influence of surface tension on the effective stiffness of nanosize plates. In: Doklady Physics. Vol. 54, pp. 98–100.

Eremeyev, V.A., Rosi, G., Naili, S., 2016. Surface/interfacial anti-plane waves in solids with surface energy. Mech. Res. Commun. 74, 8–13.

Eremeyev, V.A., Rosi, G., Naili, S., 2019. Comparison of anti-plane surface waves in strain-gradient materials and materials with surface stresses. Math. Mech. Solids 24 (8), 2526–2535.

Eremeyev, V.A., Rosi, G., Naili, S., 2020. Transverse surface waves on a cylindrical surface with coating. Internat. J. Engrg. Sci. 147, 103188.

Facconi, L., Conforti, A., Minelli, F., Plizzari, G.A., 2015. Improving shear strength of unreinforced masonry walls by nano-reinforced fibrous mortar coating. Mater. Struct. 48 (8), 2557–2574.

Facconi, L., Lucchini, S.S., Minelli, F., Plizzari, G.A., 2023. Analytical model for the in-plane resistance of masonry walls retrofitted with steel fiber reinforced mortar coating. Eng. Struct. 275, 115232.

Facconi, L., Minelli, F., Lucchini, S., Plizzari, G., 2020. Experimental study of solid and hollow clay brick masonry walls retrofitted by steel fiber-reinforced mortar coating. J. Earthq. Eng. 24 (3), 381–402.

Gattesco, N., Boem, I., Dudine, A., 2015. Diagonal compression tests on masonry walls strengthened with a gfrp mesh reinforced mortar coating. Bull. Earthq. Eng. 13 (6), 1703–1726.

Gurtin, Morton E., Ian Murdoch, A., 1975. A continuum theory of elastic material surfaces. Arch. Ration. Mech. Anal. 57, 291–323.

Gurtin, M.E, Murdoch, A.I., 1976. Effect of surface stress on wave propagation in solids. J. Appl. Phys. 47 (10), 4414–4421.

Gurtin, Morton E., Murdoch, A. Ian, 1978. Surface stress in solids. Int. J. Solids Struct. 14 (6), 431–440.

Kouris, L., Alexandros, S., Triantafillou, T.C., 2018. State-of-the-art on strengthening of masonry structures with textile reinforced mortar (TRM). Constr. Build. Mater. 188, 1221–1233.

Kushch, V.I., Mogilevskaya, S.G., Stolarski, H.K., Crouch, S.L., 2013. Elastic fields and effective moduli of particulate nanocomposites with the Gurtin–Murdoch model of interfaces. Int. J. Solids Struct. 50 (7–8), 1141–1153.

Lu, T.Q., Zhang, W.X., Wang, T.J., 2011. The surface effect on the strain energy release rate of buckling delamination in thin film–substrate systems. Internat. J. Engrg. Sci. 49 (9), 967–975.

Lucchini, S.S., Facconi, L., Minelli, F., Plizzari, G., 2020. Retrofitting unreinforced masonry by steel fiber reinforced mortar coating: uniaxial and diagonal compression tests. Mater. Struct. 53 (6), 1–22.

Lucchini, S.S., Facconi, L., Minelli, F., Plizzari, G.A., 2023. Experimental and numerical evaluation of the out-of-plane bending behavior of masonry walls retrofitted by steel fiber reinforced mortar coating. Procedia Struct. Integr. 44, 2206–2213.

Masiani, R., Trovalusci, P., 1996. Cosserat and Cauchy materials as continuum models of brick masonry. Meccanica 31, 421–432.

Messali, F., Metelli, G., Plizzari, G., 2017. Experimental results on the retrofitting of hollow brick masonry walls with reinforced high performance mortar coatings. Constr. Build. Mater. 141, 619–630.

Mogilevskaya, S.G., Zemlyanova, A.Y., Kushch, V.I., 2021. Fiber-and particle-reinforced composite materials with the Gurtin–Murdoch and Steigmann–Ogden surface energy endowed interfaces. Appl. Mech. Rev. 73 (5), 050801.

Nasedkin, A.V., Kornievsky, A.S., 2019. Numerical investigation of effective moduli of porous elastic material with surface stresses for various structures of porous cells. Wave Dyn. Mech. Phys. Microstruct. Metamater.: Theor. Exp. Methods 217–228.

Nazarenko, L., Stolarski, H., Altenbach, H., 2016. Effective properties of short-fiber composites with Gurtin–Murdoch model of interphase. Int. J. Solids Struct. 97, 75–88.

Preethi, K., Raghu, P., Rajagopal, A., Reddy, J.N., 2018. Nonlocal nonlinear bending and free vibration analysis of a rotating laminated nano cantilever beam. Mech. Adv. Mater. Struct. 25 (5), 439–450.

Salerno, G., De Felice, G., 2009. Continuum modeling of periodic brickwork. Int. J. Solids Struct. 46 (5), 1251–1267.

Sevil, T., Baran, M., Bilir, T., Canbay, E., 2011. Use of steel fiber reinforced mortar for seismic strengthening. Constr. Build. Mater. 25 (2), 892–899.

Shaat, M., Mohamed, S.A., 2014. Nonlinear-electrostatic analysis of micro-actuated beams based on couple stress and surface elasticity theories. Int. J. Mech. Sci. 84, 208–217.

Shabdin, M., Attari, N.K.A., Zargaran, M., 2018. Experimental study on seismic behavior of un-reinforced masonry (URM) brick walls strengthened with shotcrete. Bull. Earthq. Eng. 16 (9), 3931–3956.

Shiva, K., Raghu, P., Rajagopal, A., Reddy, J.N., 2019. Nonlocal buckling analysis of laminated composite plates considering surface stress effects. Compos. Struct. 226, 111216.

Simoncello, N., Zampieri, P., Gonzalez-Libreros, J., Pellegrino, C., 2019. Experimental behaviour of damaged masonry arches strengthened with steel fiber reinforced mortar (SFRM). Compos. Part B: Eng. 177, 107386.

Stefanou, I., Sulem, J., Vardoulakis, I., 2008. Three-dimensional Cosserat homogenization of masonry structures: elasticity. Acta Geotech. 3, 71–83.

Steigmann, D.J., Ogden, R., 1999. Elastic surface–substrate interactions. Proc. R. Soc. Lond. Ser. A Math. Phys. Eng. Sci. 455 (1982), 437–474.

Sun, C.-T., Achenbach, J.D., Herrmann, G., 1968. Continuum theory for a laminated medium.

Trovalusci, P., Masiani, R., 2003. Non-linear micropolar and classical continua for anisotropic discontinuous materials. Int. J. Solids Struct. 40 (5), 1281–1297.

Wang, G., He, Z., Chen, Q., 2021. The surface effects on solid and hollow nanowires under diametral loading. Appl. Math. Model. 96, 697–718.

Wang, C., Sarhosis, V., Nikitas, N., 2018. Strengthening/retrofitting techniques on unreinforced masonry structure/element subjected to seismic loads: A literature review. Open Constr. Build. Technol. J. 12 (1), 251–268.

Wang, J., Zhuping, H., Duan, H., Shouwen, Y., Feng, X., Gangfeng, W., Zhang, Weixu, Wang, T., 2011. Surface stress effect in mechanics of nanostructured materials. Acta Mech. Solida Sin. 24 (1), 52–82.

Yu, J., Park, J., 2020. Investigation of steel fiber-reinforced mortar overlay for strengthening masonry walls by prism tests. Appl. Sci. 10 (18), 6395.

Zampieri, P., Simoncello, N., Libreros, J.G., Pellegrino, C., 2020. Bond behavior of steel fiber-reinforced mortar (SFRM) applied onto masonry substrate. Arch. Civ. Mech. Eng. 20 (3), 1–20.

Zhao, X.J., Rajapakse, R.K.N.D., 2013. Elastic field of a nano-film subjected to tangential surface load: Asymmetric problem. Eur. J. Mech. A Solids 39, 69–75.

Zvolinskii, N.V., Shkhinek, K.N., 1984. Continual model of laminar elastic medium. Mech. Solids 19 (1), 1–9.